



Nanoscale

**Redox-Switchable Host-Guest Complexes of Metallocenes
and [8]Cycloparaphenylene**

Journal:	<i>Nanoscale</i>
Manuscript ID	NR-ART-07-2022-003852.R1
Article Type:	Paper
Date Submitted by the Author:	27-Aug-2022
Complete List of Authors:	Kwon, Hyejin; University of Colorado Boulder, College of Engineering and Applied Science Newell, Brian; Colorado State University, Chemistry Department Bruns, Carson J.; Univ Colorado, ATLAS Institute

SCHOLARONE™
Manuscripts

Cite this: DOI: 00.0000/xxxxxxxxxx

Redox-Switchable Host-Guest Complexes of Metallocenes and [8]Cycloparaphenylene[†]

Hyejin Kwon,^a Brian Newell^b and Carson J. Bruns^{ac*}

Received Date

Accepted Date

DOI: 00.0000/xxxxxxxxxx

The cycloparaphenylene (CPP) nanocarbons are an appealing family of macrocyclic organic semiconductors with size-tunable structures and unique optoelectronic properties, which can be further modulated by complexation with guest molecules. While many π - π -stabilized CPP-fullerene host-guest complexes are known, CPPs can also host polycyclic guests stabilized by aromatic CH- π interactions. Here we combine experimental and computational results to report that CH- π interaction can also be tapped to include redox-active metallocene guests in [8]cycloparaphenylene ([8]CPP). Oxidation of a metallocene guest is accompanied by an increase in binding affinity and tilt angle. Crystallographically determined solid-state structures of reveal CH- π interactions in the ferrocene complex (Fc \subset [8]CPP) and additional π - π interactions in the cobaltocenium complex (CoCp₂⁺ \subset [8]CPP). Functionalizing Fc with oxygen-bearing side chains also improves complex stability to a similar extent as oxidation, due to the formation of CH-O hydrogen bonds with the host's *p*-phenylene units. This work shows that CH- π bonding can be generalized as a driving force for CPP host-guest complexes and combined with other supramolecular forces to enhance stability. Owing to their semiconducting nature, amenability to functionalization, and reversible redox-dependent behavior, the [8]CPP-metallocene host-guest complexes may expand the library of synthons available for designing bespoke nanoelectronics and artificial molecular machines.

1 Introduction

Decades of research in supramolecular chemistry has yielded countless revolutionary materials ranging from nanoscale sensors¹ and machines² to large-scale plastics and elastomers with switchable, recyclable, self-healing, and/or energy-harvesting properties.³ Among the simplest and most well-defined supermolecules are inclusion or host-guest complexes,⁴ whose complementary pairwise binding motifs resemble conceptually the lock-and-key model of enzymes and substrates.⁵ Host-guest chemistry has long served as a platform for rationally probing how non-covalent bonding interactions influence molecular self-assembly processes⁶⁻⁸ and emerging properties.⁹⁻¹¹ Host-guest complexes often display rich stereochemical, dynamic, mechanical, and stimulus-responsive properties, with applications embracing chemical stabilization,¹² selective synthesis,¹³ dynamic soft materials and actuators,¹⁴ and biomedicine.¹⁵ Furthermore,

host-guest complexes are often employed to template the synthesis of molecules with topological and mechanical entanglements, known as mechanical bonds,¹⁶ which have played an essential role in the design and synthesis of artificial molecular machines.^{17,18}

Cycloparaphenylenes (CPPs) are fully π -conjugated macrocyclic hydrocarbon semiconductors that have emerged in recent years as promising nanomaterials for optoelectronic¹⁹⁻²² and supramolecular²³⁻²⁵ applications. First synthesized by Jasti²⁶ in 2008, *n*CPPs are now prepared on multigram scales and carried ([5]CPP-[12]CPP) by commercial suppliers.²⁷ In addition to binding many fullerenes via π - π interactions,²⁵ [*n*]CPPs and other carbon nanorings can be driven to form CH- π stabilized host-guest complexes, including a macrocyclic oligoanthracene-fullerene complex,²⁸ nested [*n*]CPPs,^{29,30} pyridinium \subset dimethoxy-[8]CPP,³¹ corannulene \subset [4]cyclochrysenylene,³² diquat \subset [9]CPP,³³ triquinoline \subset [12]CPP,³⁴ and a variety of polycyclic aromatic hydrocarbon (PAH)-[*n*]CPP complexes.³⁵ CH- π bonding is common in molecular crystals³⁶ and protein folding,³⁷ but not often the main interaction stabilizing a host-guest complex. Here we exploit CH- π interactions to self-assemble 1:1 complexes of [8]CPP hosts and metallocene-based guests.

Metallocenes are accessible, reliable, and reversible redox switches³⁸ with many commercial derivatives and ap-

^aDepartment of Mechanical Engineering, University of Colorado, Boulder, 427 UCB, 1111 Engineering Drive, Boulder, CO 80309.

^bMaterials and Molecular Analysis Center, Analytical Resources Core, Colorado State University, 200 W. Lake Street, Fort Collins, CO 80523

^cATLAS Institute, 1125 18th St. 320 UCB, Boulder, CO 80309, E-mail: carson.brunns@colorado.edu

[†] Electronic Supplementary Information (ESI) available: [details of any supplementary information available should be included here]. See DOI: 00.0000/00000000.

plications.^{39,40} Metallocenes have been integral to a number of ground-breaking electrochemically addressable artificial molecular machines.^{41–43} Several types of host molecules have been identified for various metallocenes,⁴⁴ including cyclodextrins,^{45–47} cucurbiturils,^{48,49} calixarenes,^{50–52} pillar[6]arenes,^{53,54} and bipyridinium-based cyclophanes.^{55–57} However, these hosts are predominantly insulating in nature, unlike the semiconducting CPPs. By identifying a CPP host for ferrocene (Fc) and cobaltocene (CoCp₂) model systems, we aim to lay a foundation for self-assembling materials that combine the advantageous redox-switching properties of metallocenes with the appealing optoelectronic properties of cycloparaphenylenes.

2 Materials and methods

2.1 Materials

[8]CPP (TCI America, 95%), ferrocene (Sigma Aldrich, 98%), bis(cyclopentadienyl)cobalt(III) hexafluorophosphate (Sigma Aldrich, 98%), ferrocene-1,1'-dicarboxaldehyde (Biogene organics, Inc., 97%), 1,1'-ferrocenedimethanol (Ambeed, 97%), tetraethyleneglycol (Alfa Aesar, 99%), and sodium azide (Sigma Aldrich, 99%) were purchased from commercial suppliers and used as-received.

2.2 Instrumentation

NMR spectroscopy was performed on a Varian 400 MHz NMR spectrometer. Raman spectroscopy was performed on a Horiba LabRAM HR Evolution Spectrometer equipped with a 100 mW 532 nm frequency-doubled Nd:YAG laser. MALDI-TOF mass spectrometry was performed on Bruker Microflex LRF. Cyclic voltammetry was performed using a three-electrode configuration including a non-aqueous reference electrode (BASi, MF-2052, Ag/AgCl (3M NaCl) Reference Electrode), Pt working electrode (BASi, MF-2013, 1.6 mm Diameter, 99.95% purity) and Pt wire auxiliary electrodes in a voltammetry cell (BASi, MF-1052). Single crystal X-ray diffraction data were acquired on a Bruker D8 QUEST diffractometer equipped with a Photon50 CMOS detector and curved graphite monochromator using Mo K α radiation ($\lambda = 0.71073 \text{ \AA}$).

2.3 DFT Calculations

DFT calculations were performed with *Gaussian 16* software on the RMACC Summit Supercomputer.⁵⁸ Geometry optimizations were performed using various functionals (LC-BLYP, B97X, LC- ω PBE, CAM, B3LYP) with the 6-311G(d) basis set and counterpoise corrections of basis set superposition errors (BSSE). All stationary points were optimized without symmetry assumptions and characterized at the same level of theory. The calculated energy-minimized structures were visualized and analyzed with Avogadro and Mercury software packages.

2.4 Host-Guest Titration Procedures

A solution of metallocene guest ($0.4 - 25 \times 10^3 \text{ M}$) was added in aliquots to a solution of [8]CPP ($0.4 - 1.2 \times 10^3 \text{ M}$) at $20 \text{ }^\circ\text{C}$ in deuterated solvents. The mixture was agitated for 10 s in a vortex

mixer. The changes in the chemical shift of a guest and [8]CPP were monitored as a function of the added a guest by ¹H NMR spectroscopy. The continuous variation method was applied to a series of solutions of [8]CPP and Fc with variable molar ratios at a total concentration of 2.0 mM in CDCl₃ for characterization by ¹H NMR spectroscopy.

2.5 Binding Constant Calculations

Chemical shift and concentration data at each point in the titration were uploaded to the free web-based Bindfit platform maintained by Pall Thordarson (<http://supramolecular.org/>) and fit using a 1:1 binding model and the Nelder-Mead search algorithm.^{59,60}

2.6 Variable Temperature NMR (VT-NMR).

The ¹H NMR probe was cooled via the controlled evaporation of liquid nitrogen in the presence of flowing nitrogen gas to avoid possible oxidation of probe electronic components. The temperature was lowered in $10 \text{ }^\circ\text{C}$ increments and the sample was equilibrated at each temperature for at least 5 minutes before taking scans.

2.7 Raman Spectroscopic Analysis

The samples were prepared by drop-casting on a microslide. The data were collected at three different spots from 100 cm^{-1} to 1800 cm^{-1} with 600 gr/mm of grating, 10% ND filter.

2.8 MALDI-TOF Mass Spectrometry

A matrix solution of α -cyano-4-hydroxycinnamic acid (α -HCCA) in 70% acetonitrile and 30% water solution (1 mg/ml) or dithranol in chloroform (1 mg/ml) was used. Pepcal II (0.7 kDa-3.5 kDa) was used as a calibrant. 1-3 μl of each sample were transferred to a MALDI plate and then 1-3 μl of the matrix solution was applied on top of each well. The samples were air-dried before MALDI-MS analysis. At least 4–5 spectra were collected from different spots across each substrate in reflector mode. The data were processed using Bruker MALDI Biotyper software.

2.9 Cyclic Voltammetry

The electrode surface was cleaned with polish before each measurement. [8]CPP solution (1 mg in 0.1 ml of CH₂Cl₂), Fc solution (10 mg in 3.3 ml of CH₂Cl₂) and Fc/[8]CPP solution (Fc:[8]CPP = 1:10) were prepared and drop-cast on the center of electrode in 2- μl increments and air dried. The drop-casting procedure was repeated 10 times. Scans were recorded with the electrodes submerged in degassed 0.3 M NaCl from -0.95 V to $+0.1 \text{ V}$ at scan rates of 50, 100, or 200 mV/s.

2.10 X-ray Crystallography

Structures were determined for the compounds listed in Table S1. Single crystals were coated with Paratone-N oil and mounted under a cold stream of nitrogen. Initial lattice parameters were obtained from a least-squares analysis of more than 100 reflections; these parameters were later refined against all data. None of the

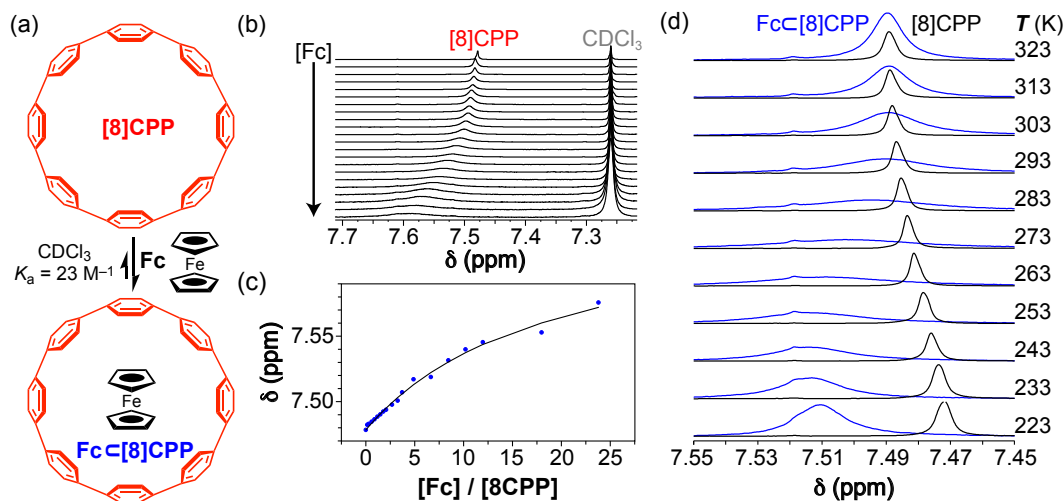


Fig. 1 $\text{FcC}[8]\text{CPP}$. (a) Schematic self-assembly of $\text{FcC}[8]\text{CPP}$. (b) ^1H NMR titration (400 MHz, 293K, CDCl_3) showing the change in chemical shift of the $[8]\text{CPP}$ (1.1 mM) signal with increasing $[\text{Fc}]$ (0 – 26.9 mM). (c) Example binding isotherm based on the NMR titration ($K_a = 23 \text{ M}^{-1}$, averaged over 2 trials). (d) Partial VT ^1H NMR spectrum (400 MHz, CDCl_3) of free $[8]\text{CPP}$ (dark grey) and a 2:1 $\text{Fc}:[8]\text{CPP}$ mixture (2 mM, blue).

crystals showed significant decay during data collection. Data were integrated and corrected for Lorentz and polarization effects using Bruker APEX4 software, and semiempirical absorption corrections were applied using SCALE.⁶¹ Space group assignments were based on systematic absences, E statistics, and successful refinement of the structures. Structures were solved using Direct Methods and were refined with the aid of successive Fourier difference maps against all data using the SHELXTL 6.14 software package.⁶² Thermal parameters for all non-hydrogen atoms were refined anisotropically. All hydrogen atoms were assigned to ideal positions and refined using a riding model with an isotropic thermal parameter 1.2 times that of the attached carbon atom (1.5 times for methyl hydrogens). Selected bond distances and angles for crystals of the $\text{FcC}[8]\text{CPP}$ and $\text{CoCp}_2\text{PF}_6\text{C}[8]\text{CPP}$ complexes are collected in Table S1. All other metric parameters can be found in the cif files included with the Supporting Information. Definitions of R1 and wR2. $R1 = \sum ||F_o| - |F_c|| / \sum |F_o|$; $wR2 = \sum [w(F_o^2 - F_c^2)^2] / \sum [w(F_o^2)]^{1/2}$.

3 Results and discussion

3.1 Self-Assembly of $\text{FcC}[8]\text{CPP}$

We selected $[8]\text{CPP}$ as a potential host for Fc because its cavity appears to be size- and shape-complementary with the surface of Fc. The $[8]\text{CPP}$ ^1H NMR signal broadens and shifts upfield by up to 0.12 ppm (Fig. 1b). Non-linear regression analysis (Fig. 1c) of the ^1H NMR titration data against a 1:1 binding model in the Bindfit web application^{59,60} gave an association constant of $29 \pm 12 \text{ M}^{-1}$ (averaged over three trials) at 20 °C. The binding constant was 40 M^{-1} in single trials at 40, 30, and 10 °C, indicating that the self assembly is dominated by ΔH and ΔS is relatively small. In the 1:1 $\text{Fc}:[8]\text{CPP}$ mixture, the $[8]\text{CPP}$ signal shifts further upfield as the temperature is lowered (Fig. 1d), but the hosts and guests remain in fast exchange, since the complexed and non-complexed signals were not split even at 223 K. On the other hand, the Fc ^1H NMR signal broadens and shifts to slightly higher

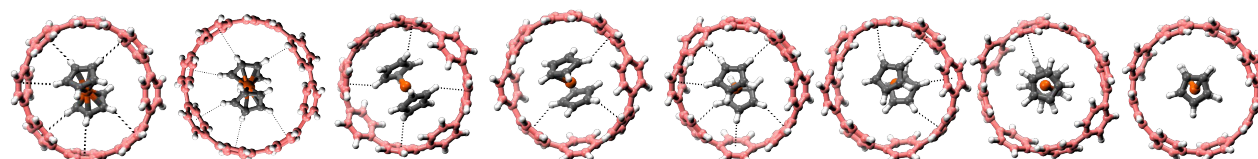
frequency (+0.01 ppm) when mixed with $[8]\text{CPP}$. The relatively small changes in chemical shift, which reflect the low binding constant, have also been observed in some CPP-fullerene host-guest complexes.⁶³ These changes in chemical shift are consistent with CH- π interactions, where the Fc guest directs some protons into the phenylene units of the $[8]\text{CPP}$ host. Although the continuous variation method (Job plot) is no longer considered a reliable technique for estimating host-guest stoichiometry,^{60,64} the Job plot is also consistent with a 1:1 complex (Fig S1a).^{63,65} The ultraviolet spectra show isosbestic points (Fig. S1b) at 320 and 365 nm as Fc is titrated into a solution of 8CPP.

The 1:1 $\text{FcC}[8]\text{CPP}$ complex has also been observed in the gas phase by MALDI-TOF mass spectrometry (Fig S1b), with a $[M]^+$ signal at $m/z = 793.306$ (Figure S1b). A more pronounced $[M-\text{Cp}]^+$ signal can also be observed at $m/z = 729.332$. In the solid-state, the Raman signals (Fig. S2) of $[8]\text{CPP}$ exhibit changes when hosting an Fc guest. The intensity of the squeezing motion of the nanohoop mode at 495 cm^{-1} decreases and shifts to higher wavenumber when $[8]\text{CPP}$ hosts an Fc guest, while the band intensity at $1175\text{--}1225 \text{ cm}^{-1}$ (in-plane CH bend) increases and the band at $1240\text{--}1290 \text{ cm}^{-1}$ (inter-ring CC stretch) decreases. These spectral changes indicate complexation-induced changes in the bond lengths and dihedral angles of $[8]\text{CPP}$, where (i) a lengthened C1-C1' bond and (ii) more relaxed dihedral angle (promoting the outward C-H bending mode) indicate an increase in aromatic character (Fig. S3).

3.2 Solid-State Structure of $\text{FcC}[8]\text{CPP}$

We grew single crystals of the $\text{FcC}[8]\text{CPP}$ complex by solvent evaporation in CHCl_3 and determined the solid-state structure by X-ray diffraction (XRD) analysis (Fig. 2). The unit cell of the crystal contains two $\text{FcC}[8]\text{CPP}$ complexes (Fig. 2a) whose central Fe atoms are offset by 13.637 \AA . The dihedral angles of the $[8]\text{CPP}$ rings are summarized in Fig. S4. In each of the complexes, the Cp planes of the Fc guest are tilted at an average angle of $\sim 47^\circ$

Table 1 Comparison of the CH- π and π - π bonding parameters in the single-crystal structure of FcC[8]CPP and the energy-minimized gas-phase structures calculated with the M062X, wB97X, LC-BLYP, LC- ω PBE, CAMB3LYP, and B3LYP DFT functionals and the 6-311G(d) basis set.



	XRD Structure	M062X	wB97X	LCBLYP	LC ω PBE	CAMB3LYP	B3LYP	
ΔE (kcal/mol)	-2.16	-2.16	-22.4	-14.8	-9.3	-5.1	-4.3	-3.7
Tilt Angle ($^\circ$)	45.6	49.0	69.6	62.5	47.8	31.4	14.7	0.9
# of CH- π Bonds	6	6	4	3	6	4	1	0
Avg. d_{PLN} (Å)	2.94 ± 0.08	2.92 ± 0.09	2.67 ± 0.05	2.79 ± 0.06	2.81 ± 0.04	2.78 ± 0.01	2.96 ± 0.00	-
Avg. $\angle_{\text{C-H-X}}$ ($^\circ$)	137.8 ± 16.1	137.8 ± 16.1	126.8 ± 4.0	130.3 ± 6.4	136.6 ± 18.4	150.7 ± 10.6	161.4 ± 0.00	-
# of π - π Bonds	0	0	2	2	1	0	0	0
Avg. $\angle_{\pi_m-\pi_n}$ ($^\circ$)	-	-	17.2	20.0	28.8	-	-	-
Avg. $d_{\pi_m-\pi_n}$ (Å)	-	-	3.770	4.106	4.313	-	-	-

(45.6° and 49.0°) with respect to the plane of the [8]CPP cavity, such that six phenylene rings in [8]CPP engage in CH- π interactions with six of the sp^2 -hybridized cyclopentadienyl (Cp) protons in Fc. The presence of these CH- π interactions were identified using both the Brandl-Weiss⁶⁶ and Nishio CHPI⁶⁷ systems, each of which set geometric cut-offs for interatomic distances and angles in CH- π bonds (see Fig. S5a-b). The CH- π bonds in each complex have an average H-to-plane distance, d_{PLN} , of ~ 2.9 Å and an average C-H-X bond angle, $\angle_{\text{C-H-X}}$, of $\sim 138^\circ$, where "X" represents the centroid of the π -donating phenylene ring. No π - π interactions⁶⁸ (see Fig. S5c) were detected between the host and guest in this complex. A comparison (Fig. S3) of [8]CPP's C-C bond lengths in the free macrocycle⁶⁹ and the FcC[8]CPP complex shows that the complexed [8]CPP exhibits increased aromatic character, with relatively longer C1-C1' bonds and shorter C1-C2/C2-C3 bonds, consistent with the Raman spectral shifts in Fig. S2. A stacking plot of the complexes (Fig. 2b) shows a herringbone packing pattern, with a stacking distance between Fe centers of 6.506 Å and a tilt angle of 44.7° between the planes of CPP cavities in adjacent columns. This type of packing is commonly observed in the solid-state superstructures of uncomplexed [n]CPP crystals,⁷⁰ including that of [8]CPP.⁶⁹

3.3 Gas-Phase DFT Calculations

In order to make predictions about related [8]CPP-metallocene host-guest complexes, we validated a method to predict the energy-minimized superstructure of the FcC[8]CPP complex using density functional theory (DFT). The geometry optimizations were performed with the 6-311G(d) basis set and initiated from the crystallographic structure of the complex using a variety of functionals, especially dispersion-corrected functionals designed for supramolecular systems.⁷¹ The results of these calculations using B3LYP,⁷² LC-BLYP,⁷³ CAM-B3LYP,⁷⁴ LC- ω PBE,⁷⁵ B97X,⁷⁶ and M062X⁷⁷ functionals are compared in Table 1. The B3LYP and CAM functionals converge on structures where the Cp planes of Fc are nearly parallel to the plane of the [8]CPP cavity, whereas they are more orthogonal in the case of the B97x and M062X functionals so as to engage in π - π interactions with the pheny-

lene rings of [8]CPP. Only the LC-BLYP and LC- ω PBE calculations converged on structures similar to the observed solid-state structure with a $\sim 45^\circ$ tilt of the Fc unit's Cp planes relative to plane of the [8]CPP cavity. The fact that the optimized geometries exhibit a wide range of different orientations for the Fc guest suggest that it can likely sample many nearly iso-energetic co-conformations (also known as local minima or metastable states) in the gas phase and in solution, akin to a ball in a ball bearing. This expected rapid tumbling motion is consistent with the VT ^1H NMR spectra which do not show signal splitting even at 223 K.

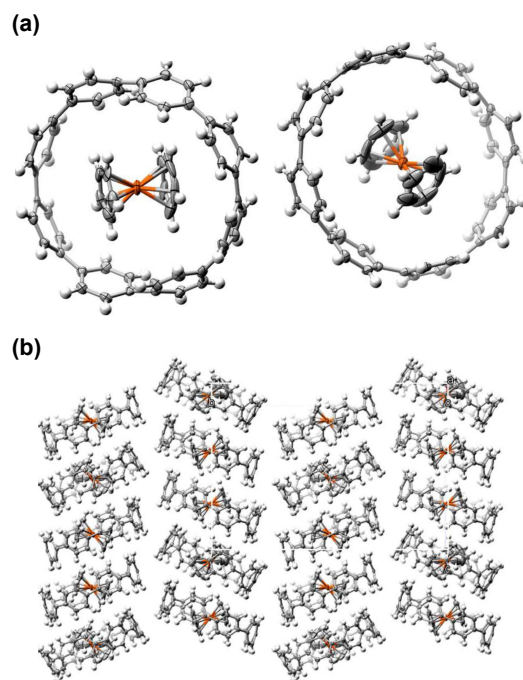


Fig. 2 Single-crystal structure of FcC[8]CPP. Solvent molecules have been removed for the sake of clarity. Thermal ellipsoids are scaled to include 50% probability. (a) The orientation of the two FcC[8]CPP complexes that make up the asymmetric monoclinic unit cell. (b) Packing plot that shows the alternating columns of FcC[8]CPP complexes and their tilt with respect to each other.

The LC-BLYP functional most accurately captured the solid-state geometry of $\text{Fc}\subset[8]\text{CPP}$, with a 47.8° tilt angle and six $\text{CH}-\pi$ bonds ($d_{\text{PLN}} = 2.81 \pm 0.04 \text{ \AA}$, $\angle_{\text{C-H-X}} = 136.6 \pm 18.4^\circ$) in good agreement with the XRD structure. One very weak $\pi-\pi$ interaction within the specified geometric cut-offs⁶⁸ was also observed in this superstructure. The structural differences between free $[8]\text{CPP}$ and Fc -complexed $[8]\text{CPP}$, indicating increased aromatic character in the complex, were also captured at this level of theory ($\Delta I_{\text{exp}} = \Delta I_{\text{calc}} = -0.011$ for $\text{Fc}\subset[8]\text{CPP}$, Fig. S3). The association energy ΔE_{gas} was calculated with each method after BSSE corrections. All methods predict a stable complex, but with a wide range of values for the calculated enthalpic energies ΔE_{gas} of association.

3.4 Cyclic Voltammetry

Since Fc is a well-known reversible redox switch,³⁸ we interrogated the $\text{Fc}\subset[8]\text{CPP}$ complex electrochemically using cyclic voltammetry (Fig. 3). Thin films of 1:10 $\text{Fc}:[8]\text{CPP}$ mixtures were drop cast from DCM on a platinum working electrode, dried, and submerged in N_2 -purged aq. NaCl (0.3 M) with a Ag/AgCl reference electrode and a Pt counter electrode. At a scan rate of 50 mV/s, two redox waves are observed; one at 0.18 V corresponds to that of uncomplexed Fc , while the second reversible wave centered at 0.30 V can be ascribed to the $\text{Fc}\subset[8]\text{CPP}/\text{Fc}^+\subset[8]\text{CPP}$ redox couple. No major changes were observed at higher scan rates of 100 and 200 mV/s (Fig. S6). Over the course of repeated scans (Fig. 3b), the Fc/Fc^+ signals are depleted more rapidly than the $\text{Fc}\subset[8]\text{CPP}/\text{Fc}^+\subset[8]\text{CPP}$ signals, likely because the water-insoluble $[8]\text{CPP}$ hosts suppress the extraction of complexed Fc^+ ions into the aqueous electrolyte compared to the water-soluble free Fc^+ ions. Based on peak-fitting analysis (Fig. S7), the $\text{Fc}^+:\text{Fc}^+\subset[8]\text{CPP}$ ratio decreases from 1.9:1 to 1.4:1 over three scans.

3.5 Self-Assembly of $\text{CoCp}_2^+\subset[8]\text{CPP}$

Since the CV data suggests that Fc^+ maintains affinity for $[8]\text{CPP}$, we assembled and characterized an $[8]\text{CPP}$ -cobaltocenium (CoCp_2^+) complex (Fig. 4). We employ CoCp_2^+ as a surrogate for Fc^+ because it is diamagnetic, and therefore more amenable to ^1H NMR spectroscopic analysis than the paramagnetic Fc^+ ion. We determined an association constant of 450 M^{-1} by ^1H NMR titration (Fig. 4b-c) in 1:5 $\text{CD}_3\text{CN}:\text{CDCl}_3$, as CoCp_2^+ was not soluble in neat chloroform.⁵³ In the VT ^1H NMR spectrum (Fig. 4d), the CoCp_2^+ signal attributable to the complex broadens and shifts to lower frequency as the temperature is lowered, unlike the overlaid signal of uncomplexed CoCp_2^+ . As in $\text{Fc}\subset[8]\text{CPP}$, the C-H stretching band at $1175\text{--}1225 \text{ cm}^{-1}$ (C-H bending) increases slightly and the inter-ring C-C stretch at $1240\text{--}1290 \text{ cm}^{-1}$ decreases when $[8]\text{CPP}$ hosts CoCp_2^+ , while the G band ($1560\text{--}1620 \text{ cm}^{-1}$) shifts to lower wavenumber (Fig. S8). In the MALDI mass spectrum (Fig. S9a), we observed a $[\text{M}-\text{Cp}]^+$ signal (common in metallocenes), as well as $[\text{M}-\text{H}]^+$ and $[\text{M}-2\text{H}]^+$ signals attributable to laser induced coalescence, as observed in prior CPP complexes.^{35,78}

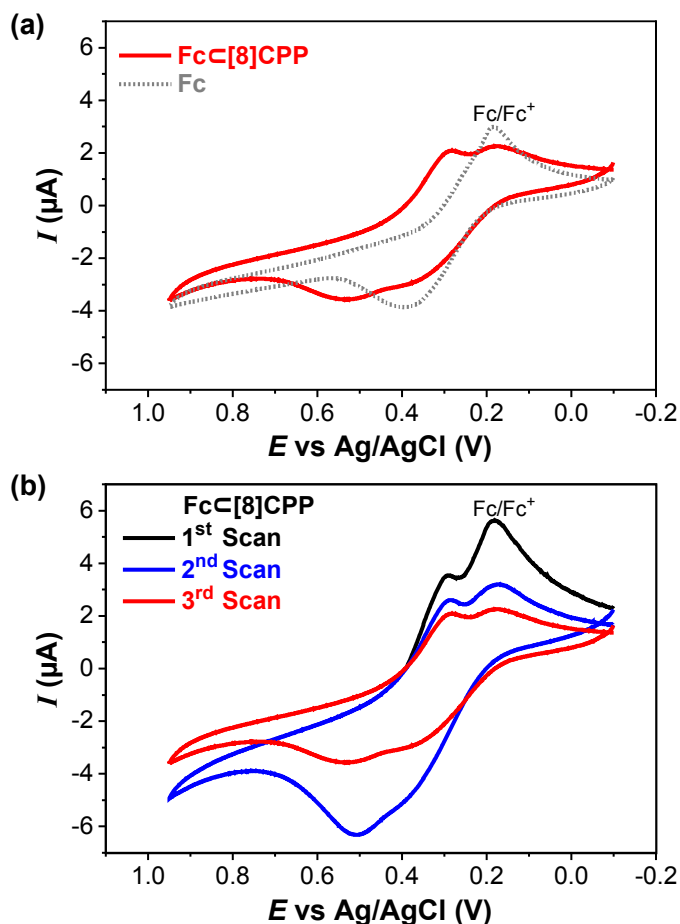


Fig. 3 Cyclic voltammograms (scan rate 50 mV/s, 0.3M aq. NaCl) of thin films drop-cast on a Pt working electrode against an aq. Ag/AgCl reference electrode and a Pt counter electrode. (a) Comparison of pure Fc with a 1:5 ratio of $\text{Fc}:[8]\text{CPP}$ mixture. (b) Three repeat scans of a $\text{Fc}:[8]\text{CPP}$ mixture shows that the signals attributable to free Fc are depleted more rapidly than the signals attributable to the $\text{Fc}\subset[8]\text{CPP}$ complex, presumably due to differences in their extraction efficiency into the aqueous electrolyte.

3.6 Solid-State Structure of $\text{CoCp}_2^+\subset[8]\text{CPP}$

We grew single crystals of $\text{CoCp}_2^+\subset[8]\text{CPP}$ complex by slow evaporation of a $\text{CHCl}_3/\text{CH}_3\text{CN}$ (5:1, v/v) solution. Like $\text{Fc}\subset[8]\text{CPP}$, the unit cell of the $\text{CoCp}_2^+\text{PF}_6\subset[8]\text{CPP}$ crystal contains two complexes. Unlike $\text{Fc}\subset[8]\text{CPP}$, these two complexes exhibit substantially different tilt angles (76.5° and 88.3°) for the Cp planes of the guest with respect to the plane of the $[8]\text{CPP}$ cavity. Thus, the oxidized metallocenium guest differs from the neutral one in its tilt angle with respect to $[8]\text{CPP}$ by $30\text{--}40^\circ$ in the solid state. The high tilt angles allow the CoCp_2^+ guest to engage in $\pi-\pi$ interactions with the phenylene units of the $[8]\text{CPP}$ host in both cases, with offset angles ($\angle_{\pi_m\pi_n}$) of 8.8° and 24.4° and centroid-to-centroid distances (d_{mn}) of 3.868 and 3.944 \AA , well below the 4.4 \AA cutoff considered for $\pi-\pi$ interactions (Fig. S5c).⁶⁸ One of the unit cell's complexes (88.3° tilt) has only two strong $\pi-\pi$ bonds, while the other complex (76.5° tilt) has two $\text{CH}-\pi$ bonds accompanying its two slightly weaker (longer bondlength) $\pi-\pi$ interactions. A different packing pattern (Fig. 5b) is observed in the XRD superstructure of $\text{CoCp}_2^+\text{PF}_6\subset[8]\text{CPP}$

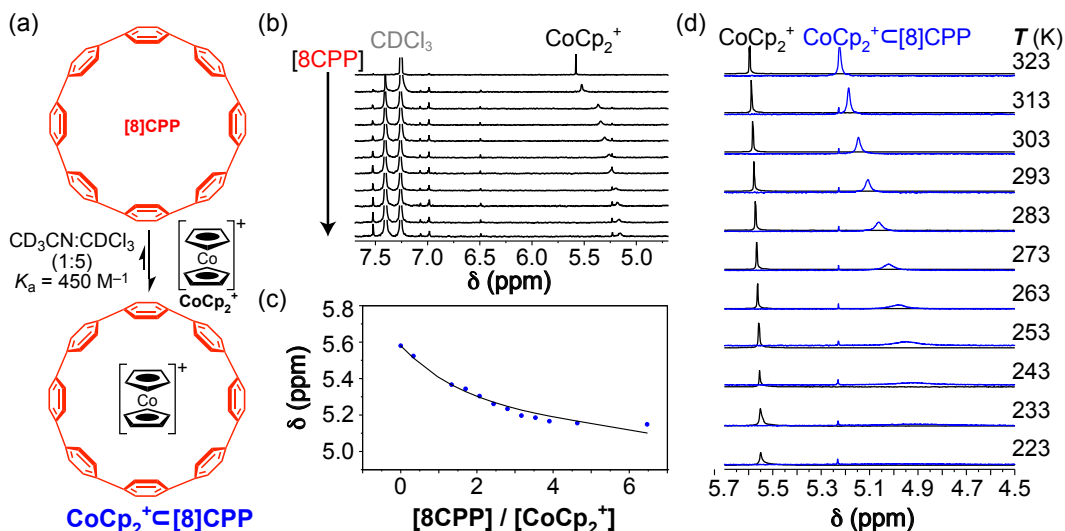


Fig. 4 $\text{CoCp}_2^+ \subset [8]\text{CPP}$. (a) Schematic self-assembly of $\text{CoCp}_2^+ \subset [8]\text{CPP}$. (b) ^1H NMR titration (400 MHz, 293K, 1:5 $\text{CD}_3\text{CN}:\text{CDCl}_3$) showing the change in chemical shift of the CoCp_2^+ (0.25 mM) signal with increasing $[8]\text{CPP}$ (0 - 1.65 mM). (c) Example binding isotherm based on the NMR titration ($K_a = 450 \text{ M}^{-1}$, averaged over 2 trials). (d) The partial VT ^1H NMR spectra (400 MHz, 1:5 $\text{CD}_3\text{CN}:\text{CDCl}_3$) of CoCp_2^+ (dark grey) and 1:1 $\text{CoCp}_2^+:[8]\text{CPP}$ (blue) become increasingly different as the temperature is lowered from 323 K to 223 K.

compared to the herringbone packing of $\text{Fc} \subset [8]\text{CPP}$. In this case, the $[8]\text{CPP}$ rings pack in alternating rows with nearly orthogonal orientations, and two PF_6 counterions occupy the interstices between complexes in every other row. The dihedral angles in the $[8]\text{CPP}$ rings of the $\text{CoCp}_2^+ \cdot \text{PF}_6 \subset [8]\text{CPP}$ complexes do not vary as widely as they do in free $[8]\text{CPP}$ and $\text{Fc} \subset [8]\text{CPP}$ (Figure S4), which is supportive of the stabilizing π - π interactions in the former. The Cp ring radius and the Cp-to-Cp distance in Fc and CoCp_2^+ each differ by $<0.05 \text{ \AA}$; their nearly identical size suggests that sterics are not responsible for the difference in tilt angle.

We repeated the DFT method comparison for the gas-phase $\text{CoCp}_2^+ \subset [8]\text{CPP}$ complex (Table S2). In this case, the converged structures are more similar than in the case of $\text{Fc} \subset [8]\text{CPP}$, with tilt angles ranging from 45.8° – 68.4° , all of which fall below the two experimentally observed angles of 76.5° and 88.3° in the solid state. In the crystal, both Cp rings of the guest engage in π - π interactions with the $[8]\text{CPP}$ host, yet most of the calculated structures show only one π - π interaction, with the exception of M062X. Thus, the solid-state superstructure of $\text{CoCp}_2^+ \subset [8]\text{CPP}$ most closely resembles the gas-phase superstructure predicted with the M062X functional, which had the highest tilt angle and two π - π interactions. The M062X functional has been employed previously to predict other types of π - π stabilized CPP host-guest complexes.^{79,80} All of the DFT methods we employed predict that $\text{CoCp}_2^+ \subset [8]\text{CPP}$ is more stable than $\text{Fc} \subset [8]\text{CPP}$, but only the LC- ω PBE and CAMB3LYP functionals predict major differences ($>10^\circ$) in host-guest tilt angle between the complexes of Fc and CoCp_2^+ .

3.7 Functionalized Fc Guests for $[8]\text{CPP}$

The use of $\text{Fc} \subset [8]\text{CPP}$ in functional materials such as porous frameworks or mechanically interlocked molecules may require the Fc core to be functionalized. In order to deter-

mine if $[8]\text{CPP}$ could also host bis-functionalized ferrocenes ($\text{Fc}(\text{R})_2$) (Fig. 6a), we evaluated the binding affinity of two guests: 1,1'-ferrocenedialdehyde ($\text{Fc}(\text{CHO})_2$) and bis-(2-

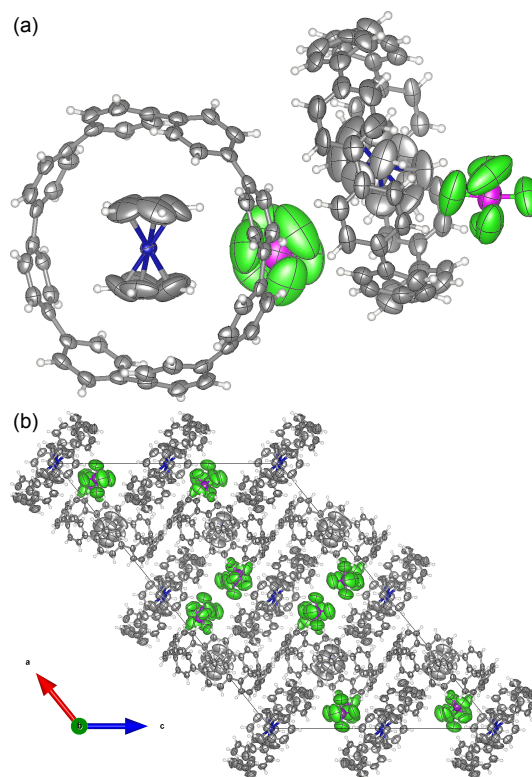
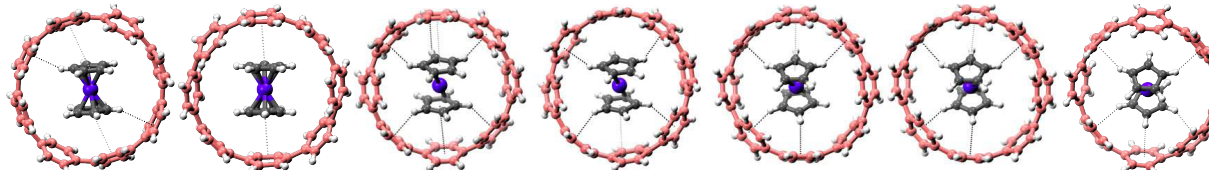


Fig. 5 Single-crystal structure of $[\text{CoCp}_2 \subset [8]\text{CPP}]\text{PF}_6$. Thermal ellipsoids are scaled to include 50% probability. (a) The orientation of the two $\text{CoCp}_2^+ \subset [8]\text{CPP}$ complexes that make up the asymmetric monoclinic unit cell. (b) Packing plot shows alternating rows of orthogonally positioned complexes with pairs of PF_6 counterions occupying the interstices between complexes one of the two types of rows.

Table 2 Comparison of the CH- π and π - π bonding parameters in the single-crystal structure of $\text{CoCp}_2^+\text{C}[8]\text{CPP}$ and the energy-minimized gas-phase structures calculated with the M062X, wB97X, LC-BLYP, LC- ω PBE, and CAMB3LYP DFT functionals and the 6-311G(d) basis set.



	Exp	M062X	wB97X	LCBLYP	LC ω PBE	CAMB3LYP	
ΔE (kcal/mol)	-3.5	-3.5	-36.3	-28.9	-24.6	-19.2	-17.7
Tilt Angle ($^\circ$)	76.5	88.3	68.4	60.3	45.8	45.9	46.5
# of CH- π Bonds	2	-	4	4	4	4	5
Avg. d_{PLN} (\AA)	2.798	-	2.67 ± 0.08	2.76 ± 0.05	2.66 ± 0.07	2.72 ± 0.05	2.77 ± 0.04
Avg. $\angle_{\text{C-H-X}}$ ($^\circ$)	157.9	-	127.6 ± 4.5	130.6 ± 9.6	134.6 ± 10.7	138.2 ± 10.7	135.2 ± 8.4
# of π - π Bonds	2	2	2	1	1	1	-
Avg. $\angle_{\pi_m-\pi_n}$ ($^\circ$)	24.4	8.8	12.0 ± 12.8	13.2	24.7	25.1	-
Avg. $d_{\pi_m-\pi_n}$ (\AA)	3.868	3.944	3.797 ± 0.02	4.1	4.3	4.3	-

(2-(2-(2-azidoethoxy)ethoxy)ethoxy)methylferrocene ($\text{Fc}(4\text{EGN}_3)_2$). We estimated an association constant of $K_a = 590 \pm 310 \text{ M}^{-1}$ (averaged over two trials) for the $\text{Fc}(\text{CHO})_2$ complex by ^1H NMR spectroscopic titration (Fig. 6d-e) in CDCl_3 . As in the prior [8]CPP-metallocene assemblies, the VT ^1H NMR spectrum (Fig. 6b) of the 1:1 mixture becomes increasingly broadened and upfield-shifted at lower temperatures, while the G band Raman signals of [8]CPP also shift (Fig. S10). The much higher binding affinity of $\text{Fc}(\text{CHO})_2\text{C}[8]\text{CPP}$ compared to $\text{FcC}[8]\text{CPP}$ suggests that the aldehyde groups enable additional stabilizing non-covalent bonding interactions. Indeed, the energy-minimized gas-phase superstructure (Fig. 6c) is stabilized by two CH-O hydrogen bonding interactions between the phenylene units of the host and the aldehyde groups of the guest, as well as three of the expected CH- π interactions. Geometry optimization of four gas-phase complexes based on different energy-minimized Fc conformers (Figure S11) at the LC-BLYP/6-311G(d) level of theory predicts that $\text{Fc}(\text{CHO})_2\text{C}[8]\text{CPP}$ is substantially more stable than $\text{FcC}[8]\text{CPP}$ (in good agreement with observations), the most stable species being the *trans* isomer shown in Fig. 6c and Fig. S11.

CH-O hydrogen bonds are also important stabilizing interactions for many guests that bind cyclobis(paraquat-*p*-phenylene), where significant binding enhancements can be achieved by introducing more oxygen atoms in extended oligoether side chains.^{81,82} We looked for evidence of a similar stability enhancement with $\text{Fc}(4\text{EGN}_3)_2$. The azide termini were included to enable further modification by way of azide-alkyne cycloaddition "click" reactions in future work. The association constant of the $\text{Fc}(4\text{EGN}_3)_2\text{C}[8]\text{CPP}$ complex was determined to be $350 \pm 60 \text{ M}^{-1}$ (averaged over two trials) by ^1H NMR spectroscopic titration (Fig. 6f-g). Therefore, extended oligoether side chains do not offer significant stability enhancements over $\text{Fc}(\text{CHO})_2$. The Raman signals of [8]CPP in the $\text{Fc}(4\text{EGN}_3)_2\text{C}[8]\text{CPP}$ show slight broadening of the G band compared to free [8]CPP, while no other significant changes were observed (Fig. S12). These functionalized complexes establish the feasibility of further modifying

$\text{FcC}[8]\text{CPP}$ as a template for new materials by a variety of means (such as Wittig, imine, or click reactions) without compromising the stability of the complex.

4 Conclusions

Until now, no guest for unmodified [8]CPP has been reported, nor have metallocenes been employed as guests for *n*CPP nanorings. Employing metallocenes as guests for [8]CPP confers a degree of redox control over binding affinity and geometry, which we have confirmed both experimentally and with DFT calculations. The metallocene guests can be functionalized with oxygenated side-chains to enhance binding affinity, providing opportunities to incorporate them in functional materials in future work. The discovery of CPP-metallocene host-guest complexes thus unlocks a new family of redox-active, semiconducting synthons available for molecular machinery, molecular electronics, and organic electronic materials.

Author Contributions

C. J. B and H.K. conceived the idea and planned the experiments. H.K performed the experiments and the computational calculations. B.N performed the single crystal X-ray Diffraction analysis. All authors participated in the manuscript preparation.

Conflicts of interest

There are no conflicts to declare.

Acknowledgements

This study was partly supported by the American Chemical Society Petroleum Research Fund Doctoral New Investigator grant (59067-DNI7). Further support was provided by the College of Engineering and Applied Science at the University of Colorado Boulder. This work utilized resources from the University of Colorado Boulder Research Computing Group, which is supported by the National Science Foundation (awards ACI-1532235 and ACI-1532236), the University of Colorado Boulder, and Colorado State University. The authors acknowledge the Department of

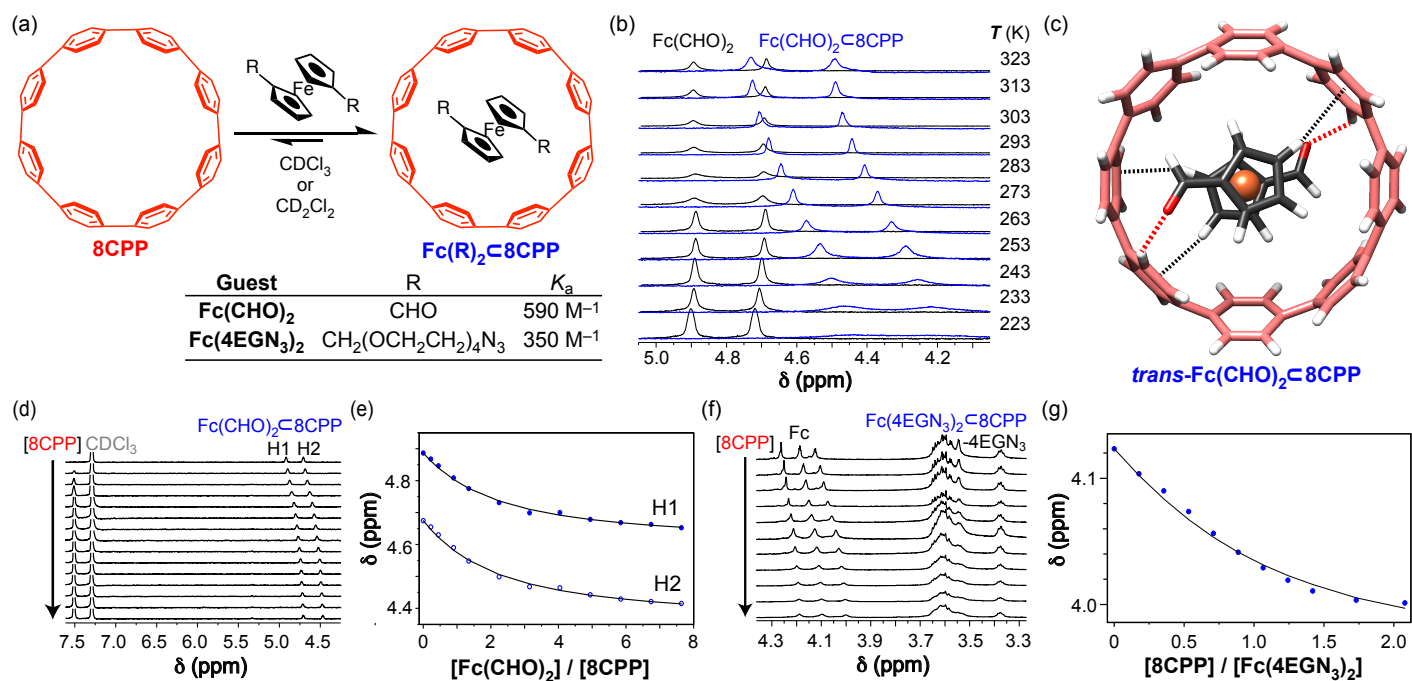


Fig. 6 Functionalized ferrocene guests for $[\text{8CPP}]$. (a) Schematic self-assembly of bis-functionalized host-guest complexes $(\text{Fc}(\text{R})_2)_2\text{C}[\text{8CPP}]$. (b) A comparison of the partial VT ^1H NMR spectra (400 MHz, CDCl_3) of free $\text{Fc}(\text{CHO})_2$ (dark grey) and 1:1 $\text{Fc}(\text{CHO})_2\text{:}[\text{8CPP}]$ (blue) reveals that they become increasingly divergent as the temperature is lowered from 323 K to 223 K. (c) Energy minimized gas-phase superstructure of the *trans*- $\text{Fc}(\text{CHO})_2\text{C}[\text{8CPP}]$ complex calculated at the LC-BLYP/6-311G(d) level of theory, with CH-O and CH- π hydrogen bonds shown as dashed red and black lines, respectively. (d) ^1H NMR titration (400 MHz, 293K, CDCl_3) showing the change in chemical shift of the $\text{Fc}(\text{CHO})_2$ (0.36 mM) signals H1 and H2 with increasing $[\text{8CPP}]$ (0 - 2.82 mM). (e) Example binding isotherm based on the NMR titration ($K_a \sim 590 \text{ M}^{-1}$). (f) ^1H NMR titration data (400 MHz, 293K, CD_2Cl_2) showing the change in chemical shift of the $\text{Fc}(\text{4EGN}_3)_2$ (3.4 mM) signal with increasing $[\text{8CPP}]$. (g) Example binding isotherm based on the NMR titration data ($K_a \sim 350 \text{ M}^{-1}$).

Chemistry and the Raman Microspectroscopy Laboratory, and at the University of Colorado Boulder for the use of NMR, UV-Vis-NIR, FL, and Raman spectroscopy instrumentation. The authors acknowledge the Materials and Molecular Analysis Center at Colorado State University for the use of MALDI-TOF-MS instrumentation. The authors thank Dr. Bimala Lama (Department of Chemistry at the University of Colorado-Boulder) for NMR support and Dr. Thomas Lee for ESI-MS (Mass Spectrometry Facility at the University of Colorado-Boulder).

Notes and references

- 1 L. You, D. Zha and E. V. Anslyn, *Chem. Rev.*, 2015, **115**, 7840–7892.
- 2 S. Erbas-Cakmak, D. A. Leigh, C. T. McTernan and A. L. Nussbaumer, *Chem. Rev.*, 2015, **115**, 10081–10206.
- 3 T. Aida, E. W. Meijer and S. I. Stupp, *Science*, 2012, **335**, 813–817.
- 4 D. J. Cram, *Angew. Chem., Int. Ed. Engl.*, 1988, **27**, 1009–1020.
- 5 D. J. Cram, *Science*, 1974, **183**, 803–809.
- 6 K. N. Houk, A. G. Leach, S. P. Kim and X. Zhang, *Angew. Chem., Int. Ed. Engl.*, 2003, **42**, 4872–4897.
- 7 M. D. Pluth and K. N. Raymond, *Chem. Soc. Rev.*, 2007, **36**, 161–171.
- 8 H.-J. Schneider and A. K. Yatsimirsky, *Chem. Soc. Rev.*, 2008, **37**, 263–277.
- 9 A. E. Kaifer, *Acc. Chem. Res.*, 1999, **32**, 62–71.
- 10 S. Allenmark, *Chirality*, 2003, **15**, 409–422.
- 11 D.-H. Qu, Q.-C. Wang, Q.-W. Zhang, X. Ma and H. Tian, *Chem. Rev.*, 2015, **115**, 7543–7588.
- 12 D. J. Cram, *Nature*, 1992, **356**, 29–36.
- 13 M. Yoshizawa, J. K. Klosterman and M. Fujita, *Angew. Chem., Int. Ed.*, 2009, **48**, 3418–3438.
- 14 A. Harada, Y. Takashima and M. Nakahata, *Acc. Chem. Res.*, 2014, **47**, 2128–2140.
- 15 X. Ma and Y. Zhao, *Chem. Rev.*, 2015, **115**, 7794–7839.
- 16 J. F. S. Carson J. Bruns, in *The Nature of the Mechanical Bond: From Molecules to Machines*, Wiley-VCH, 2016.
- 17 J. F. Stoddart, *Angew. Chem., Int. Ed.*, 2017, **56**, 11094–11125.
- 18 J.-P. Sauvage, *Angew. Chem., Int. Ed.*, 2017, **56**, 11080–11093.
- 19 E. Kayahara, L. Sun, H. Onishi, K. Suzuki, T. Fukushima, A. Sawada, H. Kaji and S. Yamago, *J. Am. Chem. Soc.*, 2017, **139**, 18480–18483.
- 20 N. Ozaki, H. Sakamoto, T. Nishihara, T. Fujimori, Y. Hijikata, R. Kimura, S. Irle and K. Itami, *Angew. Chem., Int. Ed.*, 2017, **56**, 11196–11202.
- 21 P. Della Sala, A. Capobianco, T. Caruso, C. Talotta, M. De Rosa, P. Neri, A. Peluso and C. Gaeta, *J. Org. Chem.*, 2018, **83**, 220–227.
- 22 J. Mun, J. Kang, Y. Zheng, S. Luo, H.-C. Wu, N. Matsuhisa, J. Xu, G.-J. N. Wang, Y. Yun, G. Xue, J. B.-H. Tok and Z. Bao, *Adv. Mater.*, 2019, **31**, 1903912.
- 23 D. Lu, Q. Huang, S. Wang, J. Wang, P. Huang and P. Du, *Front. Chem.*, 2019, **7**, 4559–9.
- 24 Y. Xu and M. von Delius, *Angew. Chem., Int. Ed.*, 2020, **59**, 559–573.
- 25 Y. Yang and M. Juríček, *ChemPlusChem*, 2021, 1–8.
- 26 R. Jasti, J. Bhattacharjee, J. B. Neaton and C. R. Bertozzi, *J. Am. Chem. Soc.*, 2008, **130**, 17646–17647.
- 27 M. R. Golder and R. Jasti, *Acc. Chem. Res.*, 2015, **48**, 557–566.
- 28 Y. Yamamoto, E. Tsurumaki, K. Wakamatsu and S. Toyota, *Angew. Chem., Int. Ed.*, 2018, **57**, 8199–8202.
- 29 S. M. Bachrach and Z.-C. Zayat, *J. Org. Chem.*, 2016, **81**, 4559–4565.
- 30 S. Hashimoto, T. Iwamoto, D. Kurachi, E. Kayahara and S. Yamago, *ChemPlusChem*, 2017, **82**, 1015–1020.
- 31 P. Della Sala, C. Talotta, T. Caruso, M. De Rosa, A. Soriente, P. Neri and C. Gaeta, *J. Org. Chem.*, 2017, **82**, 9885–9889.
- 32 T. Matsuno, M. Fujita, K. Fukunaga, S. Sato and H. Isobe, *Nat. Commun.*, 2018, **9**, 3779.
- 33 Á. Vidal-Vidal, E. M. Cabaleiro-Lago, C. S. Lopez and O. N. Faza, *ACS Omega*, 2018, **3**, 16976–16988.
- 34 S. Adachi, M. Shibasaki and N. Kumagai, *Nat. Commun.*, 2019, **10**, 3820.
- 35 H. Kwon and C. J. Bruns, *Nano Res.*, 2022, **15**, 5545–5555.
- 36 M. Nishio, *CrystEngComm*, 2004, **6**, 130–158.
- 37 M. Nishio, Y. Umezawa, J. Fantini, M. S. Weiss and P. Chakrabarti, *Phys. Chem. Chem. Phys.*, 2014, **16**, 12648–12683.
- 38 L. Fabbrizzi, *ChemTexts*, 2020, **6**, 22.
- 39 R. C. J. Atkinson, V. C. Gibson and N. J. Long, *Chem. Soc. Rev.*, 2004, **33**, 313–328.
- 40 M. F. R. Fouda, M. M. Abd-Elzaher, R. A. Abdelsamaia and A. A. Labib, *Appl. Organometal. Chem.*, 2007, **21**, 613–625.
- 41 A. Harada, *Acc. Chem. Res.*, 2001, **34**, 456–464.
- 42 K. Kinbara, T. Muraoka and T. Aida, *Org. Biomol. Chem.*, 2008, **6**, 1871–1876.
- 43 S. Ø. Scottwell and J. D. Crowley, *Chem. Commun.*, 2016, **52**, 2451–2464.
- 44 L. Peng, A. Feng, M. Huo and J. Yuan, *Chem. Commun.*, 2014, **50**, 13005–13014.
- 45 A. Harada and S. Takahashi, *J. Chem. Soc., Chem. Commun.*, 1984, 645–646.
- 46 T. Matsue, D. H. Evans, T. Osa and N. Kobayashi, *J. Am. Chem. Soc.*, 1985, **107**, 3411–3417.
- 47 A. Harada, Y. Hu, S. Yamamoto and S. Takahashi, *J. Chem. Soc., Dalton Trans.*, 1988, 729–732.
- 48 W. S. Jeon, K. Moon, S. H. Park, H. Chun, Y. H. Ko, J. Y. Lee, E. S. Lee, S. Samal, N. Selvapalam, M. V. Rekharsky, V. Sindelar, D. Sobransingh, Y. Inoue, A. E. Kaifer and K. Kim, *J. Am. Chem. Soc.*, 2005, **127**, 12984–12989.
- 49 A. E. Kaifer, *Acc. Chem. Res.*, 2014, **47**, 2160–2167.
- 50 L. Zhang, A. Macías, T. Lu, J. I. Gordon, G. W. Gokei and A. E. Kaifer, *J. Chem. Soc., Chem. Commun.*, 1993, 1017–1019.
- 51 M. Gómez-Kaifer, P. A. Reddy, C. D. Gutsche and

- L. Echegoyen, *J. Am. Chem. Soc.*, 1994, **116**, 3580–3587.
- 52 J. Alvarez, Y. Wang, M. Gómez-Kaifer and A. E. Kaifer, *Chem. Commun.*, 1998, 1455–1456.
- 53 W. Xia, X.-Y. Hu, Y. Chen, C. Lin and L. Wang, *Chem. Commun.*, 2013, **49**, 5085–5087.
- 54 S. Wang, C. Yao, M. Ni, Z. Xu, M. Cheng, X.-Y. Hu, Y.-Z. Shen, C. Lin, L. Wang and D. Jia, *Polymer Chem.*, 2017, **8**, 682–688.
- 55 P. R. Ashton, C. G. Claessens, W. Hayes, S. Menzer, J. F. Stoddart, A. J. P. White and D. J. Williams, *Angew. Chem., Int. Ed. Engl.*, 1995, **34**, 1862–1865.
- 56 M. Asakawa, P. R. Ashton, S. Menzer, F. M. Raymo, J. F. Stoddart, A. J. P. White and D. J. Williams, *Chem. – Eur. J.*, 1996, **2**, 877–893.
- 57 V. Balzani, J. Becher, A. Credi, M. B. Nielsen, F. M. Raymo, J. F. Stoddart, A. M. Talarico and M. Venturi, *J. Org. Chem.*, 2000, **65**, 1947–1956.
- 58 J. Anderson, P. J. Burns, D. Milroy, P. Ruprecht, T. Hauser and H. J. Siegel, PEARC17, New Orleans, LA, USA, 2017, p. 7 pages.
- 59 P. Thordarson, *Chem. Soc. Rev.*, 2011, **40**, 1305–1323.
- 60 D. B. Hibbert and P. Thordarson, *Chem. Commun.*, 2016, **52**, 12792–12805.
- 61 G. M. Sheldrick, SADABS, Program for Empirical Absorption Correction of Area Detector Data, 1996.
- 62 G. M. Sheldrick, SHELXTL, v. 6.14, 1999.
- 63 S. Hashimoto, T. Iwamoto, D. Kurachi, E. Kayahara and S. Yamago, *ChemPlusChem*, 2017, **82**, 1015–1020.
- 64 F. Ulatowski, K. Dąbrowa, T. Bałakier and J. Jurczak, *J. Org. Chem.*, 2016, **81**, 1746–1756.
- 65 C. Y. Huang, *Enzyme Kinetics and Mechanism - Part C: Intermediates, Stereochemistry, and Rate Studies*, Academic Press, 1982, vol. 87, pp. 509 – 525.
- 66 M. Brandl, M. S. Weiss, A. Jabs, J. Sühnel and R. Hilgenfeld, *J. Mol. Biol.*, 2001, **307**, 357–377.
- 67 M. Nishio, Y. Umezawa, M. Hirota and Y. Takeuchi, *Tetrahedron*, 1995, **51**, 8665–8701.
- 68 C. Janiak, *J. Chem. Soc., Dalton Trans.*, 2000, 3885–3896.
- 69 J. Xia, J. W. Bacon and R. Jasti, *Chem. Sci.*, 2012, **3**, 3018–3021.
- 70 J. B. Lin, E. R. Darzi, R. Jasti, I. Yavuz and K. N. Houk, *J. Am. Chem. Soc.*, 2019, **141**, 952–960.
- 71 S. Grimme, A. Hansen, J. G. Brandenburg and C. Bannwarth, *Chem. Rev.*, 2016, **116**, 5105–5154.
- 72 S. F. Sousa, P. A. Fernandes and M. J. Ramos, *J. Phys. Chem. A*, 2007, **111**, 10439–10452.
- 73 H. Iikura, T. Tsuneda, T. Yanai and K. Hirao, *J. Chem. Phys.*, 2001, **115**, 3540–3544.
- 74 T. Yanai, D. P. Tew and N. C. Handy, *Chem. Phys. Lett.*, 2004, **393**, 51–57.
- 75 O. A. Vydrov and G. E. Scuseria, *J. Chem. Phys.*, 2006, **125**, 234109–10.
- 76 J.-D. Chai and M. Head-Gordon, *J. Chem. Phys.*, 2008, **128**, 084106–16.
- 77 Y. Zhao and D. G. Truhlar, *Theoret. Chem. Acc.*, 2008, **120**, 215–241.
- 78 M. B. Minameyer, Y. Xu, S. Frühwald, A. Görling, M. Delius and T. Drewello, *Chem. Eur. J.*, 2020, **26**, 8729–8741.
- 79 Y.-Z. Liu, J.-B. Zhang and K. Yuan, *ACS Omega*, 2020, **5**, 25400–25407.
- 80 T. Iwamoto, Y. Watanabe, H. Takaya, T. Haino, N. Yasuda and S. Yamago, *Chem. Eur. J.*, 2013, **19**, 14061–14068.
- 81 P. L. Anelli, R. Ballardini, P. R. Ashton, V. Balzani, M. Delgado, M. T. Gandolfi, T. T. Goodnow, A. E. Kaifer, D. Philp, M. Pietraszkiewicz, L. Prodi, M. V. Reddington, A. M. Z. Slawin, N. Spencer, J. F. Stoddart, C. Vicent and D. J. Williams, *J. Am. Chem. Soc.*, 1992, **114**, 193–218.
- 82 R. Castro, K. R. Nixon, J. D. Evanseck and A. E. Kaifer, *J. Org. Chem.*, 1996, **61**, 7298–7303.